Tunable wire metamaterials for an axion haloscope

Nolan Kowitt,[1,*,†] Rustam Balafendiev,[2,†] Dajie Sun,[1,†] Mackenzie Wooten,[1]
Alexander Droster,[1] Maxim A. Gorlach,[2] Karl van Bibber,[1] and Pavel A. Belov[2]

[1]*Department of Nuclear Engineering, University of California, Berkeley, Berkeley, California 94720, USA*
[2]*ITMO University, St. Petersburg 197101, Russia*

Metamaterials based on regular two-dimensional arrays of thin wires have attracted renewed attention in light of a recently proposed strategy to search for dark-matter axions. The metamaterial-based resonator concept was specifically motivated by recent stringent predictions for the axion mass in one cosmological scenario, which are expected to improve further in the near future. When placed in the external magnetic field, such metamaterials facilitate resonant conversion of axions into plasmons near their plasma frequency. Since the axion mass is not known *a priori*, a practical way to tune the plasma frequency of metamaterial is required. In this work, we have studied a system of two interpenetrating rectangular wire lattices where their relative position is varied. The plasma frequency as a function of their relative position in two dimensions has been mapped out experimentally and compared with both a semianalytical theory of wire-array metamaterials and numerical simulations. Theory and simulation yield essentially identical results, which in turn are in excellent agreement with experimental data. Over the range of translations studied, the plasma frequency can be tuned over a range of 16%. This dynamic range is well suited for a search amply encompassing the predicted mass range of postinflation axion, enabling discovery or exclusion within a few years.

I. INTRODUCTION

Metamaterials are artificial media structured on subwavelength scales and exhibiting electromagnetic properties sometimes contrasting with those of the conventional materials [1–5]. An important class of such structures is presented by wire metamaterials based on regular two-dimensional (2D) or three-dimensional (3D) arrays of metallic wires [6–8]. In the simplest approximation, the electromagnetic properties of such materials are captured by the Drude model with the frequency-dependent permittivity [6,9]

$$\varepsilon(\nu) = 1 - \frac{\nu_p^2}{\nu^2 - j\nu\Gamma},\qquad (1)$$

where Γ measures Ohmic losses that are typically small at microwave frequencies, while ν_p is known as the *plasma frequency*. The propagation of waves at the frequencies below ν_p is strongly suppressed.

The response of wire metamaterials resembles that of an electron plasma in metals. In the latter case, however, ν_p is determined by the carrier density and cannot be modified. In contrast, the plasma frequency of a wire metamaterial is

___
*nkowitt@berkeley.edu
†These authors have equally contributed to the paper.

defined by the lattice period and radius of the wires, which makes it possible to flexibly tune the plasma frequency of such structures.

Recently, wire metamaterials have emerged in the context of ongoing searches for a hypothetical particle called the *axion*. This particle is a well-motivated candidate to constitute the dark matter of the Universe [10], the local density of which in our galactic halo is estimated to be $\rho_a \sim 0.45$ GeV/cm³. Axions are extraordinarily weakly coupled to matter and photons and thus defy detection in the conventional reactor- or accelerator-based searches. They may, however, be detected by their resonant conversion to a weak quasimonochromatic radio signal in a high-Q microwave cavity permeated by a strong magnetic field (Fig. 1), the resonant condition being that the cavity frequency equals the axion mass [11]: $h\nu = m_a c^2$. For scale, 1 GHz = 4.136 μeV.

The axion mass is poorly constrained, ranging from 10^{-9} to 10^{-3} eV [12] and, depending on the anticipated mass, different detection approaches have to be used. In the microwave-cavity dark-matter-axion search [11], the axion-photon conversion power depends on both unknown physics parameters such as the axion mass m_a and experimental parameters within the control of the operator:

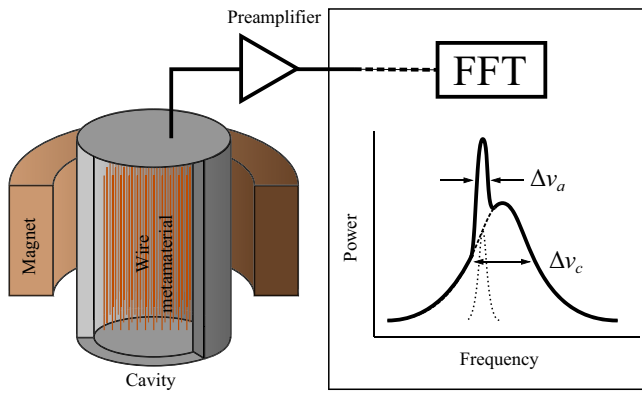$$P_{a\gamma} \propto (g_\gamma^2 \rho_a m_a)(B^2 VCQ),\qquad (2)$$

FIG. 1. A schematic of the microwave-cavity dark-matter-axion search. The cavity band pass, $\Delta\nu_c$, is determined by the quality factor of the cavity Q. The axion signal is broadened due to the virial velocity of dark matter in the Milky Way halo, $\Delta\nu_a/\nu_a \sim \beta_{\mathrm{vir}}^2 \sim 10^{-6}$. The frequency of the cavity is tuned in small steps and the power spectrum at each central frequency, calculated by a fast Fourier transform, is integrated for sufficient time to achieve the desired signal-to-noise ratio for a particular axion-photon coupling and assumed local density.

where g_γ is the dimensionless axion-photon coupling constant, of the order of unity, B is the magnetic field, and V is the cavity volume. The cavity form factor C represents the normalized squared overlap integral of the external magnetic field and the electric field of the cavity mode, a number between 0 and 1. For all current experiments, the signal will, optimistically, be of the order 10^{-23} W, putting a premium on maximizing all factors within the control of the experimentalist and exploiting state-of-the-art quantum limited or even subquantum limited receiver technology to maximize the signal-to-noise ratio [13]. A detailed treatment of the microwave-cavity technique, and a description of current experiments and their limits, have appeared in a recent review [14].

Previous and current experiments largely cluster in a little more than a decade of frequency, roughly between 0.5 and 5 GHz, which can be easily understood qualitatively. As the frequency of a cavity mode is inverse to its physical size, the lower limit on frequency is imposed by the diameter of the magnet bore in which the cavity resides. Regarding the practical upper limit of frequency, one can in principle use a smaller higher-frequency cavity in a large magnet but since the volume of a cavity goes down as the inverse third power of its linear dimension, single small cavities incur a steep penalty in the conversion power. Arrays of multiple-phased cavities and segmented cavities to maximize the utilization of magnetic volume have been attempted but are challenging from an engineering standpoint. There are also other strategies to make large-volume resonators for higher frequencies [15,16] but none have been developed for operation above 10 GHz.

Recently, Lawson *et al.* [17] have proposed a novel solution to the conundrum of how to design a resonator that can be both sufficiently large to produce a detectable signal power but for much higher frequencies than have been previously probed. In this scheme, the microwave cavity is replaced by a metamaterial consisting of a 2D lattice of wires or, equivalently, thin rods. Whereas in a conventional microwave cavity, the frequency of a mode is determined by the size of the cavity, the metamaterial is characterized by a plasma frequency, which is determined by its unit cell, a bulk property. In actual experiments, the metamaterial would reside in a metal enclosure, both to shield it from external radio-frequency noise and to maximize its quality factor Q.

In fact, the Lawson *et al.* concept [17] was inspired specifically by recent calculations of the postinflation axion mass m_a corresponding to saturation of the dark-matter density of the Universe, $\Omega_a \approx 0.27$. While the axion is allowed over several orders of magnitude in mass, there are two especially well-motivated regimes. The first is the scenario where the Peccei-Quinn symmetry breaking, which gives rise to the axion, occurs before inflation, for which the natural mass scale of the axion is in the nanoelectronvolt (approximately megahertz) range. The second, of interest here, is the scenario where Peccei-Quinn symmetry breaking occurs after inflation; in this case, the axion mass is precisely determined and, in principle, exactly calculable. The most recent estimate for the postinflation axion mass is $65 \pm 6\,\mu\mathrm{eV}$ (15.7 ± 1.45 GHz), based on supercomputer simulations of the evolution of the axion string network from the Big Bang, assuming a scale-invariant axion spectrum, which is supported by these calculations [18]. Subsequently several experiments are proposing to move upward in frequency to address the postinflation axion, among them ALPHA [19], based on a wire-array metamaterial resonator, the initial goal of which will be to cover a more ample mass range of 10–20 GHz.

The actual feasibility of wire-array metamaterials for the haloscope application is primarily defined by two factors. First, the quality factor of the cavity should be large enough to provide a sufficiently strong signal. The first experimental studies have measured quality factors around $Q \approx 220$ [20] for a wire radius of 25 μm. However, wires with a radius around 3 mm are anticipated to provide much higher quality factors $Q{\sim}4000$ in the 10 GHz range, for which the projected quality factor at cryogenic temperatures can exceed 10^4 [19].

Another crucial ingredient for the axion search is the ability to tune the array in a practical manner over a useful dynamic range in frequency, which should be at least 10%. The purpose of this study is therefore to investigate the pathways to flexibly tune the plasma frequency of the wire metamaterial. As a promising strategy, we consider a metamaterial composed of two interpenetrating wire sublattices that can be shifted relative to each other. Unlike the more intuitive tuning scheme involving changing the lattice period [21], the proposed method keeps the volume

of the structure practically constant. As we prove numerically and experimentally, the proposed strategy allows us to tune the plasma frequency of the structure up to 16% relative to the maximum frequency.

The rest of the paper is organized as follows. In Sec. II, we develop an analytical theory of metamaterials consisting of two interpenetrating wire lattices and confirm our predictions by the full-wave numerical simulations. In Sec. III, we describe our experimental results showing good agreement with our analytical predictions. Finally, in Sec. IV, we conclude the paper with a discussion of our results and an outlook.

II. ANALYTICAL AND NUMERICAL STUDIES

The plasmonic behavior of wire-array metamaterials and, specifically, their very low plasma frequency relative to that of bulk metals (approximately 10^{15} sec^{-1} in the latter case) was elucidated in an early schematic calculation of Pendry [6]. The two key factors in the schematic calculation are the greatly reduced electron density of the wire array compared to bulk metal and the dramatically increased effective electron mass due to the high magnetic field on the surface of thin wires. Together, they result in depressing the plasma frequency by many orders of magnitude.

Previously, the analytical description was developed for the wire medium based on the rectangular lattice of thin wires [9]. Below, we generalize this theory for the structure consisting of two interpenetrating wire lattices as depicted in Fig. 2. Each of the sublattices has an $a \times b$ unit cell, the cells being shifted with respect to each other by the offset vector $\boldsymbol{\Delta} = (\Delta_x, \Delta_y)$. Our goal is to calculate the plasma frequency of this metamaterial as a function of the lattice geometry governed by the parameters a, b, Δ_x, and Δ_y.
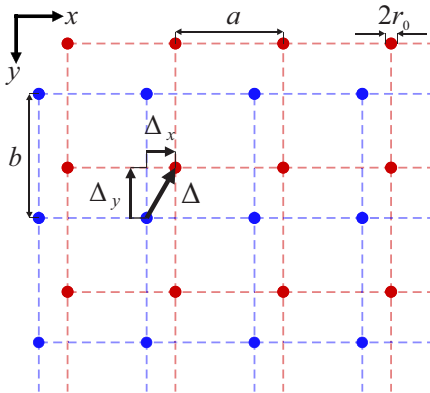

FIG. 2. A schematic of a wire medium consisting of two interpenetrating rectangular lattices with the unit-cell sizes $a \times b$ shifted with respect to each other by the vector $\boldsymbol{\Delta} = (\Delta_x, \Delta_y)$. The wire radius r_0 is assumed to be significantly smaller than the periods a and b.

In our analysis, we assume that the wires are thin, i.e., $r_0 \ll a$ and $r_0 \ll b$. Therefore, we assume that the current distribution in a wire does not depend on the azimuthal angle, which corresponds to the lowest-frequency current mode. A time-varying current $I\,e^{-jq_z z + j\omega t}$ in a single wire creates a parallel ac field given by

$$E_z = -\frac{\eta \varkappa^2}{4k} H_0^{(2)}(\varkappa R) I\, e^{-jq_z z + j\omega t}, \tag{3}$$

where the SI system of units and the $e^{j\omega t}$ time convention are adopted, $k = \omega/c$, q_z is the wave number along the axis of the wire, $\varkappa = \sqrt{k^2 - q_z^2}$, $R = \sqrt{x^2 + y^2}$, and $H_0^{(2)}$ is the Hankel function of the second kind.

The electric field produced by the wire couples to the currents in the other wires, giving rise to the collective mode. If the structure is periodic, the amplitudes of the currents obey Bloch's theorem:

$$\begin{pmatrix} I_{mn}^{(A)} \\ I_{mn}^{(B)} \end{pmatrix} = \begin{pmatrix} I^{(A)} \\ I^{(B)} \end{pmatrix} e^{-j\mathbf{q}\cdot\mathbf{R}_{mn}}, \tag{4}$$

where $I^{(A)}$ and $I^{(B)}$ denote the current amplitudes in the two sublattices.

On the other hand, since the wires are perfectly conducting, the boundary conditions require that the total electric field at the surface of the wire vanishes. Writing the total field explicitly and dividing the result by $-\eta j\,\varkappa^2/(2k)$, we recover

$$C_{\text{rec}}\, I^{(A)} + C(\boldsymbol{\Delta})\, I^{(B)} = 0, \tag{5}$$

$$C_{\text{rec}}\, I^{(B)} + C(-\boldsymbol{\Delta})\, I^{(A)} = 0, \tag{6}$$

where C_{rec} captures the contribution from the wires of the same sublattice as the wire under consideration, including its own field at the surface, and $C(\boldsymbol{\Delta})$ is responsible for the wire interaction with another sublattice.

Setting the determinant of the system in Eqs. (5) and (6) to zero, we derive the dispersion equation,

$$C_{\text{rec}} \pm \sqrt{C(\boldsymbol{\Delta})\, C(-\boldsymbol{\Delta})} = 0. \tag{7}$$

Note that the $+$ or $-$ sign choice in this equation defines the relative phase of the currents $I^{(A)}$ and $I^{(B)}$ in the two sublattices.

Here, the interaction constant for the rectangular lattice C_{rec} can be written as [9]

$$C_{\text{rec}} = \frac{1}{\pi} \ln\left(\frac{b}{2\pi r_0}\right) + \frac{1}{k_x^{(0)} b} \frac{\sin\left(k_x^{(0)} a\right)}{\cos\left(k_x^{(0)} a\right) - \cos\left(q_x a\right)}$$

$$+ \sum_{n \neq 0} \left\{ \frac{1}{k_x^{(n)} b} \frac{\sin\left(k_x^{(n)} a\right)}{\cos\left(k_x^{(n)} a\right) - \cos\left(q_x a\right)} - \frac{1}{2\pi |n|} \right\}, \tag{8}$$

where $k_x^{(n)} = -j \sqrt{\left(q_y^{(n)}\right)^2 - \varkappa^2}$ and $q_y^{(n)} = 2\pi n/b + q_y$. In expression for $k_x^{(n)}$, the sign in front of the square root is chosen such that the real part of the square root is positive.

Using the Poisson summation formula, we also derive the expression for the interaction constant of the two lattices:

$$C(\boldsymbol{\Delta}) = -\sum_{n=-\infty}^{\infty} \frac{e^{jq_y^{(n)}\Delta_y}}{k_x^{(n)}b}$$
$$\times \frac{e^{jq_x a}\sin\left(k_x^{(n)}\Delta_x\right) + \sin\left[k_x^{(n)}(a-\Delta_x)\right]}{\cos(q_x a) - \cos\left(k_x^{(n)}a\right)}. \quad (9)$$

The dispersion equation given in Eq. (7) together with the expressions for the interaction constants in Eqs. (8) and (9) fully determine the dispersion properties of the wire medium sketched in Fig. 2. However, the key parameter relevant for plasma haloscopes is the plasma frequency ν_p. It is obtained as the lowest-frequency root of the dispersion equation for the zero wave vector $\mathbf{q} = 0$. In such a case, since the wires in the two sublattices are identical, $C(-\boldsymbol{\Delta}) = C(\boldsymbol{\Delta})$, which yields

$$C_{\text{rec}} \pm C(\boldsymbol{\Delta}) = 0. \quad (10)$$

Using the identity

$$\frac{\sin\alpha}{\cos\alpha - 1} = -\cot\frac{\alpha}{2},$$

we simplify the dispersion equation further and obtain

$$\frac{1}{\pi}\ln\left(\frac{b}{2\pi r_0}\right) - \frac{1}{k_x^{(0)}b}\cot\left(\frac{k_x^{(0)}a}{2}\right)$$
$$- \sum_{n\neq 0}\left[\frac{1}{k_x^{(n)}b}\cot\left(\frac{k_x^{(n)}a}{2}\right) + \frac{1}{2\pi|n|}\right]$$
$$\mp \sum_{n=-\infty}^{\infty}\frac{\exp\left(2\pi j n\Delta_y/b\right)}{k_x^{(n)}b}\frac{\cos\left[k_x^{(n)}(a/2-\Delta_x)\right]}{\sin\left(k_x^{(n)}a/2\right)} = 0. \quad (11)$$

Here, $k_x^{(n)} = -j\sqrt{(2\pi n/b)^2 - k^2}$ and the unknown parameter is the normalized frequency $k = \omega/c$. The plasma frequency is calculated from the lowest-frequency root $k_{\min}$ of this equation as $\nu_{pl} = ck_{\min}/(2\pi)$.

To explain qualitatively why the smallest root of the dispersion equation corresponds to the plasma frequency, we note that the two lowest bands in the dispersion of the structure originate from the respective symmetric and antisymmetric modes of current in the wire dimers. Since the symmetric mode lies lower in frequency, the lowest

band originates from in-phase oscillations of current in the wires. To complement this simplified argument, we note that our analytical model captures both in-phase and out-of-phase oscillations of currents in the two sublattices and this results in + or − sign choice in the dispersion equation [see Eq. (7) and accompanying text]. We have evaluated two cases with our analytical model corresponding to measurements presented further below. For the unit cell $(a, b) = (5.88 \text{ mm}, 5.48 \text{ mm})$, the choice of sign corresponding to the symmetric mode results in frequencies between 13.05 and 15.25 GHz, for all relative positions of the two sublattices, while the other choice of sign corresponding to the antisymmetric mode yields much higher frequencies, i.e., between 55 and 63 GHz. Similarly, for the unit cell $(a, b) = (5.88 \text{ mm}, 14.12 \text{ mm})$, the symmetric mode falls in the range 7.1–9.0 GHz, whereas the antisymmetric mode lies between 21 and 25 GHz. The in-phase distribution of current in the wires is also confirmed based on the results of full-wave numerical simulations, which agree well with our analytical model.

Note also that the result for the rectangular lattice [9] is recovered from Eq. (11) by omitting the last term characterizing the interaction with another sublattice.

To explore the dependence of the plasma frequency on the parameters of the wire medium, the resulting equation has been solved numerically using the MATLAB software package for several values of r_0/a and a/b. Figure 3 shows how the plasma frequency of an infinite medium changes with the relative shift of the two sublattices. Figures 3(a) and 3(b) show the change in the frequency for the case where the ratio of the unit-cell period to the wire radius $a/r_0 = 20$. For Figs. 3(c) and 3(d), the wires are thinner: $a/r_0 = 200$. As can be seen, the cases with a rectangular sublattice unit cell $(b = 2a)$ produce a dramatic change in frequency when tuned along the wider side and hardly any change when tuned along the shorter one (Table I). The comparison of the two radii also shows that the relatively thicker wires enable greater tuning when sublattices are moved along the larger period b (i.e., in the y direction) from the position of the maximum plasma frequency. In order to verify the obtained results, the same unit cells were modeled using the COMSOL MULTIPHYSICS eigenmode solver, with the resulting discrepancy of the semianalytical results with the numerical ones being less than 0.2%.

III. EXPERIMENTAL DESCRIPTION

The experiments mapping out the dependence of the plasma frequency on the unit cell were carried out with the microwave setup depicted in Fig. 4. The 3D wire array was built up by stacking planes of regularly spaced wires; this allowed the lattice to be conveniently reconfigured by changing spacers between planes, shifting alternate planes, etc.
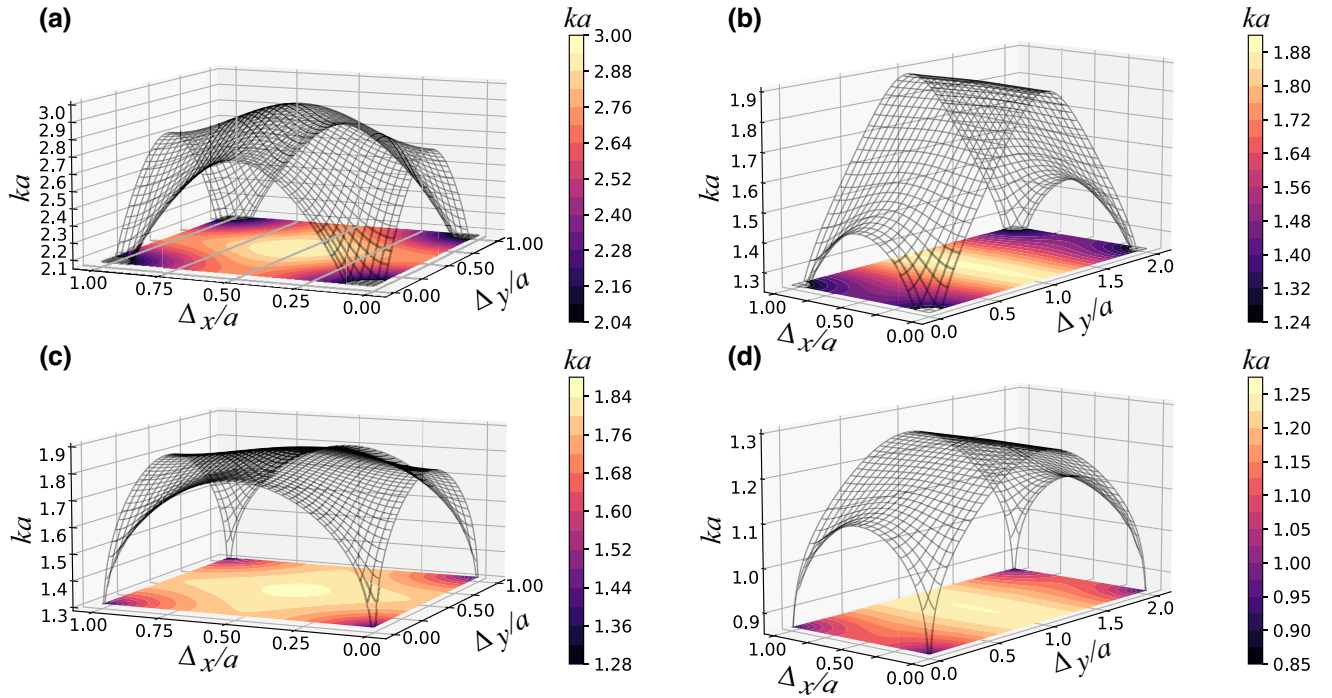
FIG. 3. The results of the semianalytical MATLAB calculations for four infinite lattices of wires. The contours and the wire-mesh surface show the normalized plasma frequency ka as a function of the relative sublattice displacement Δ_x and Δ_y. (a),(b) The results for a medium with $a/r_0 = 20$, close to the point at which the wires can no longer be considered thin. (c),(d) The change of the plasma frequency for a medium with $a/r_0 = 200$, well within the bound of our theory being applicable. The sublattices in (a) and (c) are square, with periods $b = a$, while the sublattices in (b) and (d) are elongated, so that $b = 2a$. As can be seen, for square sublattices, movement along any trajectory leads to a noticeable frequency shift. For a rectangular sublattice, however, frequency tuning mainly corresponds to movement along y, with movement along x bringing little change in frequency (see Table I below).

The wire planes, 20 in total, were constructed by fabricating square aluminum frames of 203- (254-) mm inner (outer) edge length and 1.23-mm thickness. The frames were then strung with gold-on-tungsten wires [22] of radius and spacing in the plane of $(r_0, a) = (25\,\mu\text{m}, 5.88\,\text{mm})$. The wires were glued onto a thin plastic bridge on either side of the frame, from which they were thus electrically isolated [see Fig. 5(a)].

The metamaterial parameters are extracted from the measured transmission spectra, i.e., the S_{21}, one of the four scattering parameters for a two-port device. Specifically, this is the ratio of the output of the second port relative to the input of the first port, V_2^+/V_1^+, and is conveniently expressed as the scalar logarithmic gain, $g = 20 \cdot \log_{10}(|S_{21}|)$ [dB]. Within a Drude model, the complex frequency-dependent permittivity is given by

TABLE I. The tuning percentage of the plasma frequency in the semianalytical MATLAB calculations, defined as $(\nu_{\max} - \nu_{\min})/\nu_{\max}$ for various cases illustrated in Fig. 3. The first column shows the tuning achievable by bringing the two sublattices in direct contact. The second and third columns show tuning by moving the second sublattice from the maximum frequency configuration to the edge of the unit cell along x and y, respectively.

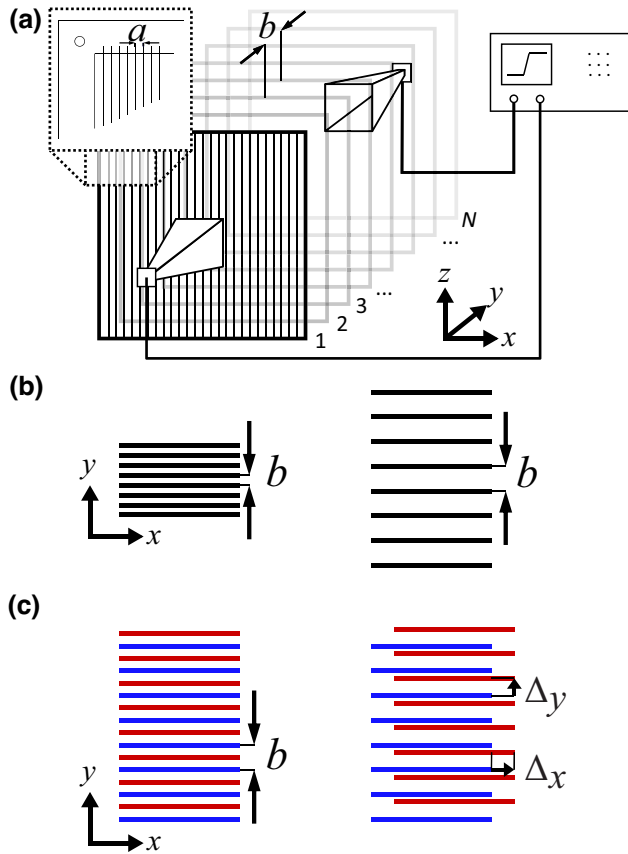| Lattice parameters	Change of (Δ_x, Δ_y)	$(a/2, b/2)$ to $(0, 2r_0)$ (%)	$(a/2, b/2)$ to $(0, b/2)$ (%)	$(a/2, b/2)$ to $(a/2, 0)$ (%)
$a/r_0 = 20, b = a$		29.2	7.5	7.5
$a/r_0 = 20, b = 2a$		33.7	0.3	22.5
$a/r_0 = 200, b = a$		29.3	2.7	2.7
$a/r_0 = 200, b = 2a$		31.0	0.1	10.9

FIG. 4.　(a) The geometry for the measurements of S_{21} for an array of N planes. The inset on the top left shows the construction of a single wire plane. The wires are supported by the metallic wire frame but are not in electrical contact with it. (b) The first set of measurements, looking at the change in plasma frequency as a function of the spacing between planes of wires b. (c) The second set of measurements, done with two sets of planes. The change in the plasma frequency is measured as a function of the relative sublattice offset $\mathbf{\Delta} = (\Delta_x, \Delta_y)$.

$\epsilon(\nu) = \epsilon'(\nu) - j\epsilon''(\nu)$, where

$$\epsilon'(\nu) = 1 - \frac{\nu_p^2}{\nu^2 + \Gamma^2} \quad \text{and} \quad \epsilon''(\nu) = \left(\frac{\nu_p}{\nu}\right)^2 \frac{\frac{\Gamma}{\nu}}{1 + (\frac{\Gamma}{\nu})^2}. \tag{12}$$

The S_{21} measurements were performed with a vector network analyzer [23] and matched waveguide horn antennas [24]. All measurements were performed in normal-incidence geometry, i.e., beam propagation perpendicular to the wire array. As the waveguide horn antennas have a beam spread of $\pm 8°$ at 3 dB, tests were performed to determine whether scattering from the inside edge of the frames was contributing to the spectra. This was done by comparing the fits with and without a rectangular collimator of microwave-absorbing material of 7.5 cm (horizontal) $\times$ 5.0 cm (vertical). No evidence was seen for scattering from the frames and thus all measurements were performed
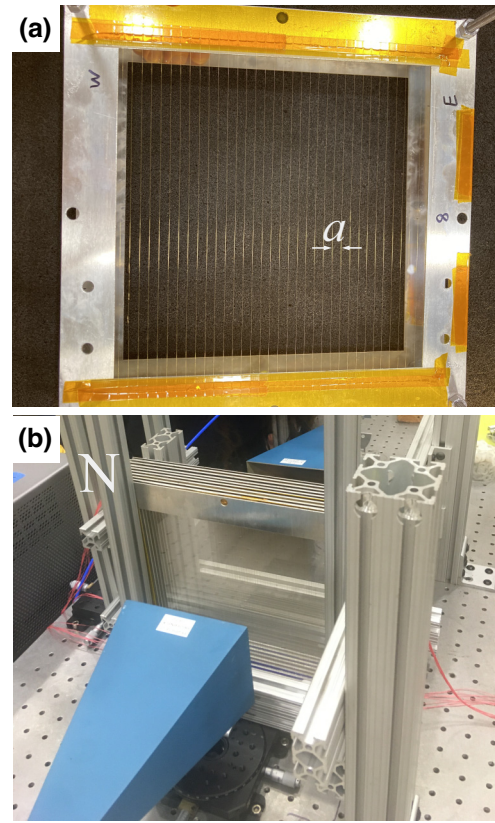
FIG. 5.　(a) The metal frame being strung with 50-μm gold-on-tungsten wires placed with a period $a = 5.88$ mm. (b) The setup for the S_{21} measurements of N planes in the close-pack configuration, i.e., without spacers.

without the collimator in place. Before and after each measurement with the wire array in place, the baseline transmission was recorded with the wire array removed; the two were averaged and then subtracted from the spectrum measured with the wire array in place to yield the S_{21} to be fitted.

The measured S_{21} spectrum is fitted with the calculated transmission through a uniform dielectric of complex permittivity ϵ' [25], returning values of ν_p, Γ, and d, with errors; for representative spectra and their fits, see Fig. 6. The sharp transition edge of the spectrum most sensitively encodes the plasma frequency ν_p and the loss term Γ; the effective width of the array d is accurately determined by the first few oscillations above the cutoff.

Extensive measurements were performed on two different methods of modifying the unit cell. The first [Fig. 4(b)] restricted the unit cell to be rectangular, maintaining the same wire spacing a in the plane but changing the spacing between the planes, b. The second [Fig. 4(c)] involved ganging alternate planes together and then translating the two groups relative to one another by an offset (Δ_x, Δ_y), i.e., a parallel and perpendicular shift. Each set of measurements will be discussed in turn.
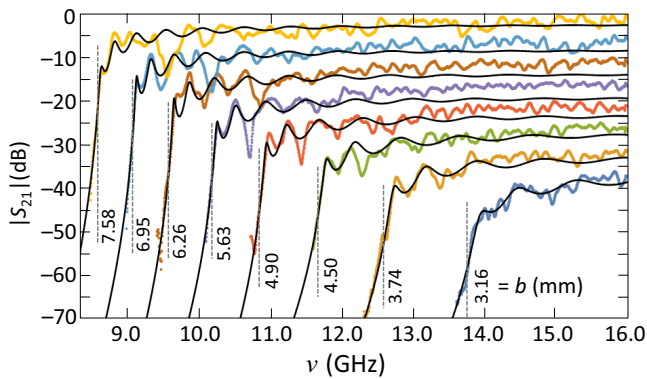
FIG. 6.   The S_{21} spectra for a rectangular lattice, where the wire spacing in the plane a is fixed and the spacing between planes b is varied. The experimental data are represented in color and the fitted calculation in black. The vertical dotted lines indicate the fitted plasma frequency for each spectrum. The spectrum for $b = 7.58$ mm corresponds exactly to the vertical scale; each subsequent spectrum is offset by -5 dB for clarity.

(i) *Varying the interplane spacing*. Measurements were made with 20 wire frames, for eight different values of the interplane spacing b, varying from 3.16 to 7.58 mm. The waveguide horn antennas were placed 48 cm apart for all measurements. The plasma frequency as a function of b is shown in Fig. 7. The blue curve represents the prediction of a semianalytical theory [9]. Note that this is an absolute prediction, with no adjustable parameters; the agreement with data is at the 1% level.

While uniformly changing the spacing between planes can produce a large dynamic range in frequency, in this case a 60% increase in frequency by decreasing the spacing from 7.6 mm to 3.2 mm, this scheme presents difficulties from the perspective of designing a practical
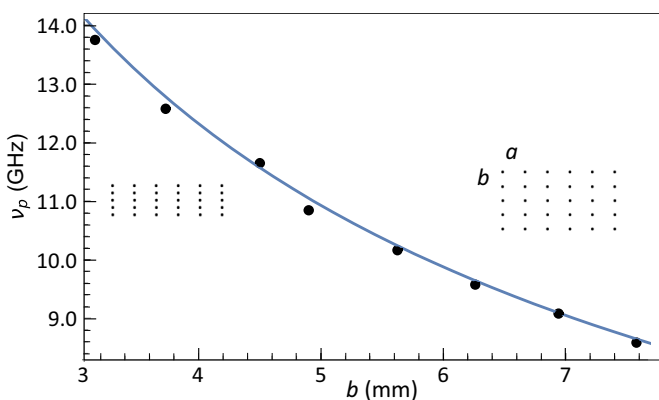

FIG. 7.   The plasma frequency for a rectangular unit cell with $a = 5.88$ mm and b variable. The ideograms, indicating larger and smaller b, are associated with lower and higher plasma frequencies, respectively. The solid dots represent data; the error bars are smaller than the symbols. The blue line represents the absolute prediction of the semianalytical theory [9].

axion haloscope. Tuning the haloscope in this manner does not conserve the volume of the active metamaterial resonator; in this example, the conversion volume is reduced by a factor of 2.4 from the lowest to highest frequency, 8.6–13.8 GHz. This represents a large loss of active volume and thus axion-plasmon conversion power, which is precisely what the plasma-haloscope concept was designed to circumvent. Furthermore, it is difficult to envision a mechanical solution by which the hermetic microwave enclosure containing the array—and which must closely conform to its boundary (roughly within a wire spacing)—can be continuously expanded and contracted as the haloscope is tuned. For a full discussion of the implementation of a wire-array metamaterial in an axion haloscope and, specifically, the integrated design of the wire array within its cavity, see Ref. [19].

(ii) *Varying the position of alternate planes*. The dependence of the plasma frequency on the unit cell was also examined by uniformly translating alternate planes of the array in directions both parallel and perpendicular to the microwave beam. Figure 2(a) depicts the coordinate (Δ_x, Δ_y) system for the translation, where Δ_x denotes the relative translation of planes parallel to one another, keeping their separation fixed, and Δ_y denotes the relative translation in the microwave propagation direction and which thus changes the relative spacing of the planes. For $(\Delta_x, \Delta_y) = (0, b/2)$, a rectangular lattice of wire spacing $(a, b/2)$ is recovered; by symmetry, one only needs to map out the unit cell from (0,0) to $(a/2, b/2)$ but extending the measurements is a valuable check on possible systematic errors. The experimental setup is shown in Fig. 5(b).

The plasma frequency ν_p was mapped out for two different lattices. Figure 8 represents the lattice $(a, b) = (5.88$ mm, 5.48 mm$)$, where the wire frames were stacked directly on top of one another, first with all the planes facing in the same direction ($\Delta_y = 2.74$ mm) and then with alternate planes facing in the opposite direction ($\Delta_y = 0.59$ mm). In the latter case, the actual planes of wires themselves come into near contact with one another; the wires are separated only by a layer of Kapton tape on top of each bridge and by a thin polyethylene sheet to protect the wires from damage as the frames were shifted relative to one another from one measurement to another. After several thousand restacking and shifting operations over the course of the project, the wires were no longer entirely taut and therefore the distribution of all wire positions relative to their fiducial location was measured on a microscope stage to determine their standard deviation along a single coordinate, $\sigma_y = 293 \mu$m. This was incorporated as a correction to the mean distance for the case of alternate places facing one another ($\Delta_y = 0.59$ mm), where the plasma frequency changes most rapidly as opposite pairs of wires approach one another. The correction is negligible at large wire separations.
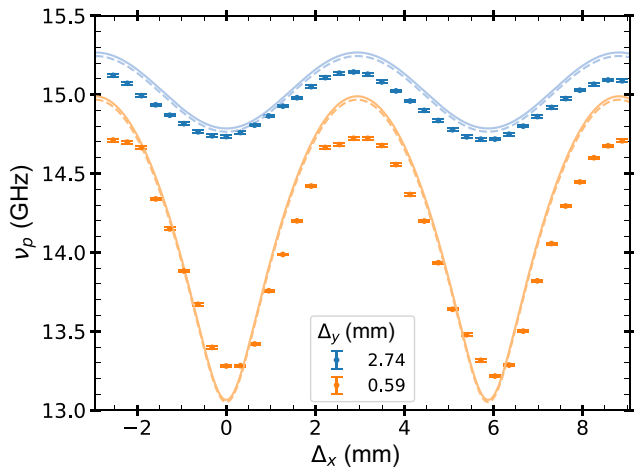
FIG. 8. The data and simulations for stacking the wire frames without spacers, $(a, b) = (5.88\ \text{mm}, 5.48\ \text{mm})$. The blue data points and curves pertain to the configuration where all the frames face in the same direction and the orange data points and curves to where alternate frames face in the opposite direction, bringing the wires into close proximity. The solid lines show semianalytical results calculated using MATLAB, while the dashed lines show numerical results calculated using COMSOL. The discrepancy between the two is less than 0.15% in both cases.

A second series of measurements was performed to map out the plasma frequencies for excursions from a larger rectangular lattice, $(a, b) = (5.88\ \text{mm}, 14.12\ \text{mm})$. The microwave horns were positioned 37 cm apart for this series. Here, alternate planes faced in opposite directions and the spacing Δ_y was adjusted in discrete steps while keeping b fixed, using a series of spacers. The transverse registration of the odd and even frames was determined by a micrometer-driven translation stage on either side of the array. Translation stages at the front and back of the array maintained the proper longitudinal dimension of the array for each measurement. This was necessary to ensure that the slight compressibility of the stack of frames and spacers did not introduce variations in Δ_y between successive measurements in Δ_x, as the array needed to be relaxed longitudinally to shift alternate planes to their new position and then recompressed for the next measurement.

In contrast with tuning the metamaterial by varying the interplane spacing, modifying the unit cell by translating alternate planes preserves the volume of the array and thus should be more amenable to implementation in an axion haloscope. (In fact, this method is not strictly volume preserving but very nearly so; over the full range of unique unit cells, the array widens by $a/2$ in the x direction and, for an even number of planes, extends by b in the y direction.) Relative to varying interplane spacing, in this case, the dynamic range is sacrificed but with the parameters explored here, the accessible frequency range would be of practical interest for the haloscope application.

The data and simulations for this configuration are shown in Fig. 9. The various combinations of spacers enabled ν_p to be mapped out in fine steps in Δ_x for five values of Δ_y, ranging from the wire planes placed close nearby ($\Delta_y = 0.59\ \text{mm}$) to equally spaced ($\Delta_y = b/2 = 7.06\ \text{mm}$). The overall agreement between data and simulations is very good, ranging from a few percent when wires are in close proximity ($\Delta_y \to 0$) to a few parts per thousand at the largest spacings ($\Delta_y \to b/2$). It is also noteworthy that the measurement and fitting of the S_{21} spectra in the latter case display the predicted oscillatory shape exactly, even for a magnitude of the oscillation as small as 10^{-3} in ν_p, lending confidence to the experimental procedure and analysis. The discrepancies in the absolute plasma frequency at larger separations can be ascribed to limitations on how accurately the plane separations
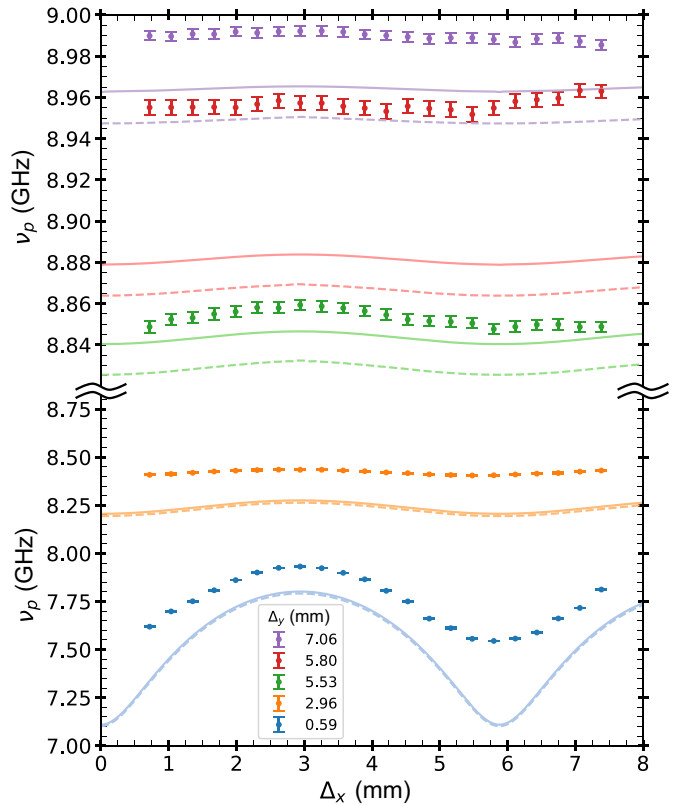

FIG. 9. The data and MATLAB simulations for profiles in Δ_x for five selected values of Δ_y, for the unit cell $(a, b) = (5.88\ \text{mm}, 14.12\ \text{mm})$. The measurements and the corresponding predictions are in the same color. Minima in the plasma frequency correspond to alignment of wires in the y direction. The solid lines show semianalytical results calculated using MATLAB, while the dashed lines show numerical results calculated using COMSOL. The resulting discrepancy of the semianalytical results with the numerical ones is less than 0.2% for all five cases. In a haloscope with a resonator of this (a, b), all values of (Δ_x, Δ_y) could be accessed, enabling coverage of all frequencies between 7.5 and 9 GHz.

TABLE II.   The tuning percentage, defined as $(\nu_{max} - \nu_{min})/\nu_{max}$, for the cases illustrated in Figs. 8 and 9. The observed tuning values are largely consistent with the results presented in Table I for $a/r_0 = 200$. The decrease in the maximum range of tuning compared to the semianalytical results is due to the range of movement along y also being significantly shorter. As can be seen, in the latter case of $b \approx 2a$ translation along y yields tuning close to the maximum possible when the wires in the two sublattices are aligned along y.

Lattice parameters	$(a/2, b/2)$ to $(0, 0.59)$ (%)	$(a/2, b/2)$ to $(0, b/2)$ (%)	$(a/2, b/2)$ to $(a/2, 0.59)$ (%)	$(0, b/2)$ to $(0, 0.59)$ (%)
$(a, b) = (5.88\text{ mm}, 5.48\text{ mm})$	12.72	2.81	2.77	9.87
$(a, b) = (5.88\text{ mm}, 14.12\text{ mm})$	16.09	0.08	11.79	16.07

Δ_y can be measured; at the smallest separation $\Delta_y = 0.59$ mm, this is compounded by slackening of the wires after repeated handling and positioning operations, which is most clearly seen in the filling in of the minima of the curves.

IV. CONCLUSIONS

In summary, our work comprehensively studies the tuning strategies for the plasma frequency of wire-medium-based metamaterials. Assuming thin wires, we develop a semianalytical theory predicting the plasma frequency for various wire lattices, which is in good agreement both with the results of full-wave numerical simulations and experiments.

We demonstrate that the plasma frequency can be flexibly reconfigured by up to 16% while keeping the volume of the metamaterial practically unchanged. Such tuning appears to be remarkable for the entire field of tunable and reconfigurable metamaterials [26–28].

Our demonstrated dynamic range in frequency is ideally suited to the search for the postinflation axion, the mass estimate of which will sharpen even further in the near future [29]. From the very first, microwave-cavity axion experiments have operated on a cadence of configuration changes by which the experiment is periodically refitted with a new cavity, tuning element, or amplifier, typically after covering 10–20% in frequency range, with each configuration running from several months to a year. The pioneering Rochester-Brookhaven-Fermilab search utilized 11 different cavity and rod combinations, with seven different amplifiers to cover 1.09–3.93 GHz [30]; HAYSTAC [13], currently in operation, requires changing out components of its two-paramplifier squeezed-state receiver approximately every 15%. Thus a metamaterial-based resonator with the dynamic range demonstrated here is entirely consistent with previous experience and covering the 10–20 GHz range around the Ref. [18] prediction for the postinflation axion represents a program of approximately four configuration changes over 5 years.

Hence, our work bridges the engineering world of metamaterials with the fundamental axion-search experiments, hopefully paving a way toward tunable wire-medium-based haloscopes for axion searches. The high tunability reported here is one of the key ingredients needed for the success of the search experiments, which may initiate further improvements in dark-matter detection.

[1] V. G. Veselago, The electrodynamics of substances with simultaneously negative values of ϵ and μ, Sov. Phys. Usp. **10**, 509 (1968).

[2] G. V. Eleftheriades and K. G. Balmain, *Negative-Refraction Metamaterials: Fundamental Principles and Applications* (John Wiley & Sons, Hoboken, New Jersey, 2005).

[3] T. Itoh and C. Caloz, *Electromagnetic Metamaterials: Transmission Line Theory and Microwave Applications* (John Wiley & Sons, Hoboken, New Jersey, 2005).

[4] R. Marqués, F. Martin, and M. Sorolla, *Metamaterials with Negative Parameters* (John Wiley & Sons, Hoboken, New Jersey, 2008).

[5] F. Capolino ed., *Theory and Phenomena of Metamaterials* (CRC Press, New York, 2009).

[6] J. B. Pendry, A. J. Holden, D. J. Robbins, and W. J. Stewart, Low frequency plasmons in thin-wire structures, J. Condens. Matter Phys. **10**, 4785 (1998).

[7] P. A. Belov, R. Marqués, S. I. Maslovski, I. S. Nefedov, M. Silveirinha, C. R. Simovski, and S. A. Tretyakov, Strong spatial dispersion in wire media in the very large wavelength limit, Phys. Rev. B **67**, 113103 (2003).

[8] C. R. Simovski, P. A. Belov, A. V. Atrashchenko, and Y. S. Kivshar, Wire metamaterials: Physics and applications, Adv. Mater. **24**, 4229 (2012).

[9] P. A. Belov, S. A. Tretyakov, and A. J. Viitanen, Dispersion and reflection properties of artificial media formed by regular lattices of ideally conducting wires, J. Electromagn. Waves Appl. **16**, 1153 (2002).

[10] J. L. Feng, Dark Matter Candidates from Particle Physics and Methods of Detection, Annu. Rev. Astron. Astrophys. **48**, 495 (2010).

[11] P. Sikivie, Experimental tests of the invisible axion, Phys. Rev. Lett. **51**, 1415 (1983).

[12] I. G. Irastorza and J. Redondo, New experimental approaches in the search for axion-like particles, Prog. Part. Nucl. Phys. **102**, 89 (2018).

[13] K. M. Backes, D. A. Palken, S. A. Kenany, B. M. Brubaker, S. B. Cahn, A. Droster, G. C. Hilton, S. Ghosh, H. Jackson, and S. K. Lamoreaux, *et al.*, A quantum enhanced search for dark matter axions, Nature **590**, 238 (2021).

[14] M. Simanovskaia, K. van Bibber, and G. Carosi, in *The Search for Ultralight Bosonic Dark Matter* (Springer, London, 2023), Chap. 4.

[15] S. Kinion, Ph.D. thesis, Department of Applied Science, University of California Davis, 2001.

[16] J. Jeong, S. Youn, S. Bae, J. Kim, T. Seong, J. E. Kim, and Y. K. Semertzidis, Search for invisible axion dark matter with a multiple-cell haloscope, Phys. Rev. Lett. **125**, 221302 (2020).

[17] M. Lawson, A. J. Millar, M. Pancaldi, E. Vitagliano, and F. Wilczek, Tunable axion plasma haloscopes, Phys. Rev. Lett. **123**, 141802 (2019).

[18] M. Buschmann, J. W. Foster, A. Hook, A. Peterson, D. E. Willcox, W. Zhang, and B. R. Safdi, Dark matter from axion strings with adaptive mesh refinement, Nat. Commun. **13**, 1049 (2022).

[19] A. J. Millar, S. M. Anlage, R. Balafendiev, P. Belov, K. van Bibber, J. Conrad, M. Demarteau, A. Droster, K. Dunne,

and A. G. Rosso, *et al.*, Searching for dark matter with plasma haloscopes, Phys. Rev. D **107**, 055013 (2023).

[20] R. Balafendiev, C. Simovski, A. J. Millar, and P. Belov, Wire metamaterial filled metallic resonators, Phys. Rev. B **106**, 075106 (2022).

[21] L. Ivzhenko, E. Odarenko, and S. I. Tarapov, Mechanically tunable wire medium metamaterial in the millimeter wave band, Prog. Electromagn. Res. Lett. **64**, 93 (2016).

[22] Luma Metall AB, Kalmar, Sweden, https://luma-metall.com/.

[23] Keysight Technologies, four-port VNA, Model E5071C, Santa Rosa, California, https://www.keysight.com/us/en/home.html.

[24] Pasternak Enterprises Electronics, WR-90 series, PE985 6B-20, Irvine, California, https://www.pasternack.com/.

[25] A. Yahalom, Y. Pinhasi, E. Shifman, and S. Petnev, Transmission through single and multiple layers in the 3–10 GHz band and the implications for communications of frequency varying material dielectric constants, WSEAS Trans. Commun. **9**, 759 (2010).

[26] M. Lapine, D. Powell, M. Gorkunov, I. Shadrivov, R. Marqués, and Y. Kivshar, Structural tunability in metamaterials, Appl. Phys. Lett. **95**, 084105 (2009).

[27] M. V. Gorkunov and M. A. Osipov, Tunability of wire-grid metamaterial immersed into nematic liquid crystal, J. Appl. Phys. **103**, 036101 (2008).

[28] A. Boardman, V. Grimalsky, Y. Kivshar, S. Koshevaya, M. Lapine, N. Litchinitser, V. Malnev, M. Noginov, Y. Rapoport, and V. Shalaev, Active and tunable metamaterials, Laser. Photon. Rev. **5**, 287 (2010).

[29] B. Safdi, Private communication.

[30] W. Wuensch, S. D. Panfilis-Wuensch, Y. Semertzidis, J. Rogers, A. Melissinos, H. Halama, B. Moskowitz, A. Prodell, W. Fowler, and F. Nezrick, Results of a laboratory search for cosmic axions and other weakly coupled light particles, Phys. Rev. D **40**, 3153 (1989).

[31] https://rscf.ru/project/23-72-10026/.